RMetS
Royal Meteorological Society

New perspectives on the collective risk of extratropical cyclones

Alasdair Hunter,[a]* David B. Stephenson,[a] Theo Economou,[a] Mark Holland[a] and Ian Cook[b]
[a]*School of Engineering, Computing and Mathematics, University of Exeter, UK*
[b]*Willis Re, London, UK*

*Correspondence to: A. Hunter, College of Engineering, Mathematics and Physical Sciences, Harrison Building, Streatham Campus, University of Exeter, North Park Road, Exeter EX4 4QF, UK. E-mail: alasdair.a.r.hunter@gmail.com

In this study, the relationship between the frequency and intensity of extratropical cyclones over the North Atlantic is investigated. A cyclone track database of extended October–March winters was obtained from the National Centers for Environmental Prediction and National Center for Atmospheric Research (NCEP–NCAR) reanalysis. A large positive correlation is found between winter cyclone counts and local sample mean vorticity over the exit region of the North Atlantic storm track in this cyclone track database. Conversely, a negative correlation is found over the Gulf Stream. Possible causes for the dependence are investigated by regressing winter cyclone counts and local sample mean vorticity on teleconnection indices with Poisson and linear models. The indices for the Scandinavian pattern, North Atlantic Oscillation and East Atlantic Pattern are able to account for most of the observed positive correlation over the North Atlantic. To consider the implications of frequency intensity dependence for the insurance industry, an aggregate risk metric was used as a proxy for the annual aggregate insured loss. Here, the aggregate risk is defined as the sum of the intensities of all events occurring within a season. Assuming independence between the frequency and intensity results in large biases in the variance and the extremes of the aggregate risk, especially over Scandinavia. Therefore including frequency intensity dependence in extratropical cyclone loss models is necessary to model the risk of extreme losses.

Key Words: clustering; extratropical cyclone; aggregate risk; NCEP–NCAR reanalysis

Received 3 March 2015; Revised 22 July 2015; Accepted 11 August 2015; Published online in Wiley Online Library

1. Introduction

In Europe, extratropical cyclones have cost tens of billions of Euros in insured losses since 1990 and quantifying the risk of further losses has been identified as being of the highest priority for the global reinsurance industry.* Modelling the risk of multiple events within a season (referred to here as the aggregate risk) of extratropical cyclones is of particular interest, due to the temporal clustering of storms in the Northern Hemisphere (Mailier *et al.*, 2006). Clusters of extratropical cyclones can result in economic losses comparable to those of a US hurricane and, due to the structure of reinsurance contracts, a cluster of events can cost more than a single event with the same total loss (Vitolo *et al.*, 2009). Climate models have been shown to underestimate clustering (Kvamstø *et al.*, 2008) and the physical drivers of clustering remains an active area of ongoing research (e.g. Hanley and Caballero, 2012; Neu *et al.*, 2013; Pinto *et al.*, 2013; Blender *et al.*, 2015). Catastrophe modelling firms have recently attempted to include clustering into their windstorm models, but as the models are not open to scrutiny it is difficult to assess how effectively this has been accomplished.†

Both Mailier *et al.* (2006) and Vitolo *et al.* (2009) have considered the implications of clustering for modelling the counts of extratropical cyclones. This study extends this to include the relation between cyclone counts and intensity. The frequency and intensity are investigated within a broader aggregate risk framework. Here the aggregate risk refers to the distribution of total intensity from the sum of all cyclone intensities in a season or year. Previous studies on hazard counts within a season, such as those of Katz (2002), Mailier *et al.* (2006) and Pinto *et al.* (2013), are a special case of the aggregate risk where the intensity is unity for each event. Aggregate risk is the main focus, due to its importance to the insurance industry for estimating the total claims that can occur in a season.

The aim of this article is to develop a flexible framework that can be used to quantify and understand the aggregate risk of extratropical cyclones. The framework is used to investigate the sensitivity of the aggregate risk to different modelling

*http://www.willisresearchnetwork.com/research-and-impact/natural-hazard-and-risk/european-windstorm.html

†http://www.air-worldwide.com/Publications/AIR-Currents/2010/European-Windstorms-Implications-of-Storm-Clustering-on-Definitions-of-Occurrence-Losses/

assumptions. This investigation will address the following main questions.

- Is there a dependence between the frequency and mean intensity of extratropical cyclones within a season/year?
- What are the physical drivers for any dependence between the frequency and intensity?
- How does frequency intensity dependence affect the distribution of aggregate losses (aggregate risk)?

2. How to model the aggregate risk

To quantify the aggregate risk from extratropical cyclones fully, one requires a measure of cyclone activity that includes both the frequency and intensity. Such a metric, called the annual aggregate loss (AAL), exists in the risk management community and is defined as the sum of the intensities (losses) for all events in a year. The distribution of the AAL can be investigated using a collective risk model (Prabhu, 1961). In this section, the basic formulation of a collective risk model is described and applied to extratropical cyclones.

Collective risk theory has its roots in the actuarial literature, dating back to the mid-twentieth century (Houston, 1960). In the collective risk model formulation, both the number of claims and the size of individual claims are assumed to be random. The AAL is therefore modelled as the sum of a random number of random variables and so it is sometimes also called the random sum model (McNeil *et al.*, 2005). Collective risk theory was developed by Filip Lundberg between 1909 and 1939; however, it was not widely adopted by the actuarial community as the relatively large amount of computational power required to apply the theory made it of little practical use (Borch, 1967). Increases in computer power allowing the implementation of techniques such as Monte Carlo simulation have resulted in collective risk theory becoming widely adopted by the insurance industry over the latter half of the twentieth century and collective risk models are now widely used in the insurance industry (Embrechts *et al.*, 1997). Collective risk theory also has the potential to be used in climate science, for example to model annual US hurricane losses (Katz, 2002) or total monthly precipitation (Katz and Parlange, 1998).

2.1. Frequency and intensity

Extremes in a single meteorological variable at a specific location can be modelled as a marked point process (Stephenson, 2008). Events occur at irregular times T_i with variable intensities X_i (see Figure 1). For natural hazards, the occurrence of events is typically modelled as a Poisson process, where $N(t)$ denotes the number of occurrences in a time interval $[0, t]$ (McNeil *et al.*, 2005). Each individual occurrence has a mark or intensity[‡] $X_1, ..X_N$. The number of occurrences N is a non-negative integer-valued random variable, while the intensities X_i are real-valued random variables. The AAL, referred to here as the aggregate risk S, is the aggregate total intensity of the N events that occur in a given time period (e.g. over a season or year):

$$S = X_1 + \cdots + X_N = \sum_{i=1}^{N} X_i.$$

The mean expected aggregate risk can be expressed using the law of total expectation by conditioning on the number of events N:

$$E[S] = E_N[\sum_{i=1}^{N} E[X_i|N]] = E[N]E[Y] + \mathrm{cov}(N, Y), \quad (1)$$

[‡]Intensity is often used to refer to the rate parameter of the Poisson distribution. In this article, intensity refers to the mark size X.

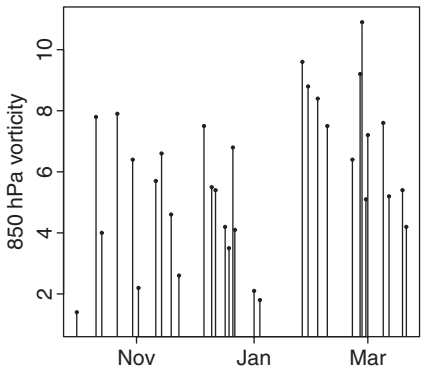

Figure 1. Time series of cyclone transits and corresponding relative vorticity (ζ_{850}) passing near Gothenburg (12.5°E, 57.5°N) between October 1989 and March 1990.

where Y is the mean intensity ($Y = \sum_{i=1}^{N} X_i/N$). The variance of the aggregate risk from the law of total variance is

$$\begin{aligned}\mathrm{var}(S) &= E_N\left[\left(\sum_{i=1}^{N} X_i|N\right)\right] + \mathrm{var}_N\left(E\left[\sum_{i=1}^{N} X_i|N\right]\right)\\ &= \mathrm{cov}(N^2, Y^2) - [\mathrm{cov}(N, Y)]^2 - 2\mathrm{cov}(N, Y)E[N]E[Y]\\ &\quad + \mathrm{var}(N)E[Y]^2 + \mathrm{var}(Y)E[N^2]\end{aligned} \quad (2)$$

(see Frishman, 1971; McNeil *et al.*, 2005).

3. Aggregate risk of extratropical cyclones

In this section, the database of storm tracks used throughout the article is introduced. The climatology of the aggregate risk for extratropical cyclones is then shown.

3.1. Data

The cyclone tracks considered here were obtained from the six-hourly reanalysis of the extended October–March winters between October 1950 and March 2003, which was produced jointly by the National Centers for Environmental Prediction and the National Center for Atmospheric Research (NCEP–NCAR reanalysis: Kalnay *et al.*, 1996; Kistler *et al.*, 2001). The mean sea-level pressure (MSLP) and the zonal and meridional 850 mb wind components were extracted. This dataset has been widely used in previous extratropical cyclone studies (e.g. Zhang *et al.*, 2004; Mailier *et al.*, 2006; Vitolo *et al.*, 2009).

An objective tracking algorithm was used on the data extracted from the NCEP–NCAR reanalysis to provide storm tracks defined at six-hourly intervals, from October 1950–March 2003 (Hodges, 1994, 1999; Hodges *et al.*, 1995). The tracking algorithm uses the following intensity variables: vorticity, sea-level pressure and maximum wind speed. In this investigation, relative vorticity ζ_{850} is used as an intensity measure that is less influenced by the background state of the atmosphere than MSLP, as it focuses on smaller spatial scales. The vorticity has also been used as the cyclone intensity measure in previous studies on extratropical cyclone risk (Mailier *et al.*, 2006; Vitolo *et al.*, 2009).

As in Vitolo *et al.* (2009) a spatial grid covering the North Atlantic and Western Europe between (125°W,40°E) in longitude and (20°N,80°N) in latitude was used to provide a set of reference points. Here, the spatial resolution was 2.5° in both longitude and latitude. At each grid point, the vorticity of cyclones as they passed within ±10° was recorded (Figure 1). Time series of the total winter counts and winter local sample mean vorticity could then be constructed for all grid points for each winter. Previous studies have typically used aggregation periods of 1 or 3 months (e.g. Vitolo *et al.*, 2009). Here, the extended winter (six-month)

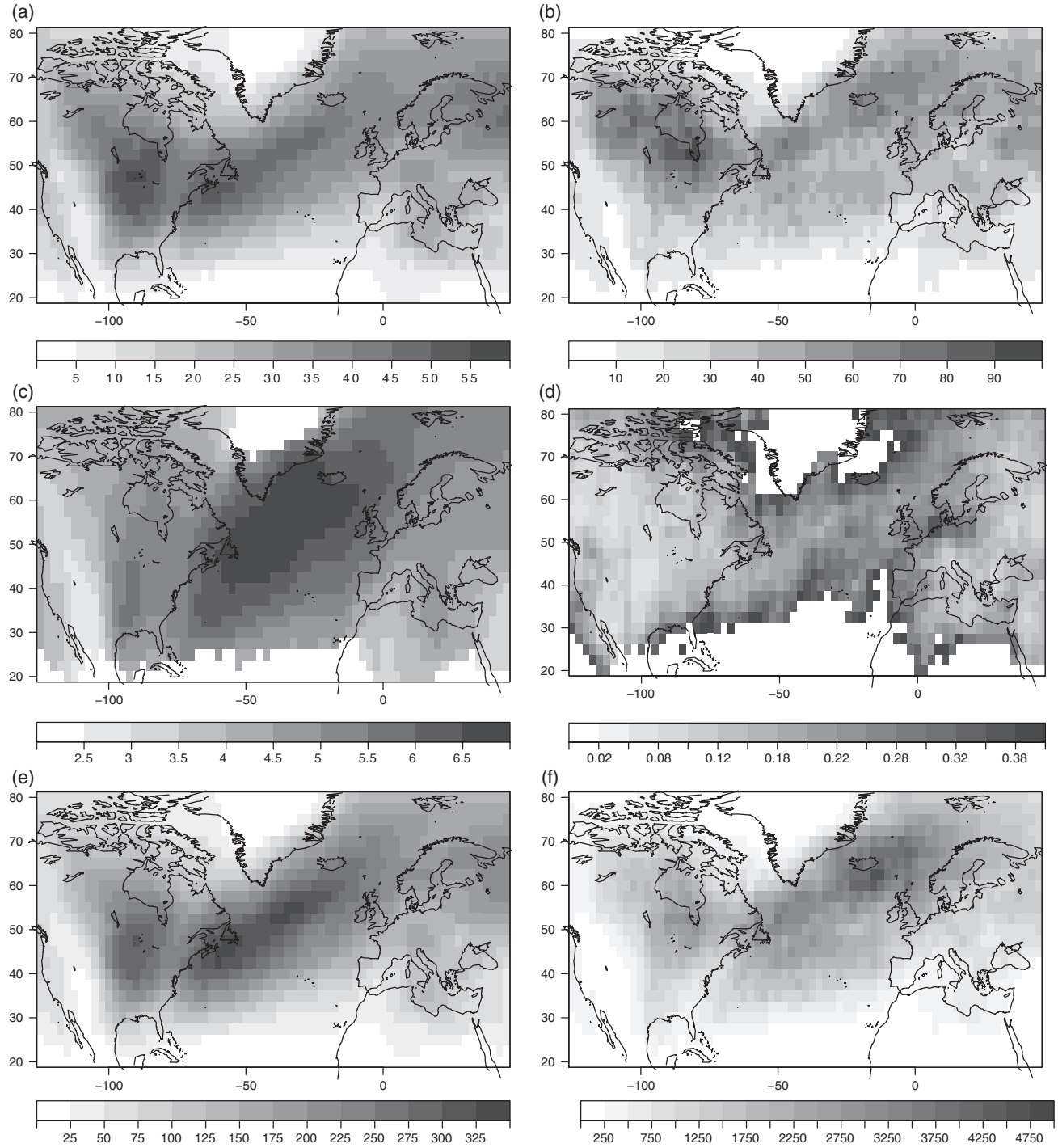

Figure 2. (a) Sample mean $\bar{n}$ cyclone counts per six-month winter, (b) sample variance s_n^2 of winter cyclone counts, (c) sample winter sample local mean vorticity $\bar{y}$, (d) sample variance s_y^2, (e) sample winter mean $\bar{s}$ of the aggregate risk and (f) sample variance s_s^2.

aggregation period is used instead, as it reflects the aggregation period of losses that would be used by an insurer.

The results of any analysis of cyclone tracks will be sensitive to the database, tracking algorithm and cyclone intensity measure used (Hodges *et al.*, 2003; Raible *et al.*, 2008; Ulbrich *et al.*, 2009; Neu *et al.*, 2013). Alternative tracking methods and intensity measures were not considered here; however, an investigation into extratropical cyclones using an alternative tracking method and intensity measure was found to produce results qualitatively similar to those of alternate studies that used Hodges algorithm and vorticity as an intensity measure (Pinto *et al.*, 2013). The spectral resolution of the NCEP–NCAR reanalysis is *T*62, which has been truncated to a total wave number of *T*42 for use with Hodges algorithm; thus filtering takes place. This filtering was investigated in Mailier (2007, section 5.7.2), where it was only found to have a noticeable impact on the cyclone counts statistic over central Asia, which is not considered in this study.

3.2. *Climatology of the aggregate risk*

The mean cyclone counts $\bar{n}$ (see Figure 2(a)) show the location of the North Atlantic storm track, agreeing with that shown in Hoskins and Hodges (2002). Areas of high cyclone activity can also be seen in the lee of the Rockies in North America. The sample variance in cyclone counts s_n^2 (Figure 2(b)) is greatest over the storm track, with the maximum towards the exit region of the storm track. These findings agree qualitatively with those of the mean and variance of monthly counts in Mailier *et al.* (2006) and the three-monthly counts in Vitolo *et al.* (2009), where both studies considered winter storm tracks from the NCEP–NCAR reanalysis.

Maxima of the sample local mean vorticity $\bar{y}$ can be noted over the North Atlantic storm track (Figure 2(c)). The variance in winter sample local mean vorticity is greatest along the north/south edges of the storm track (Figure 2(d)).

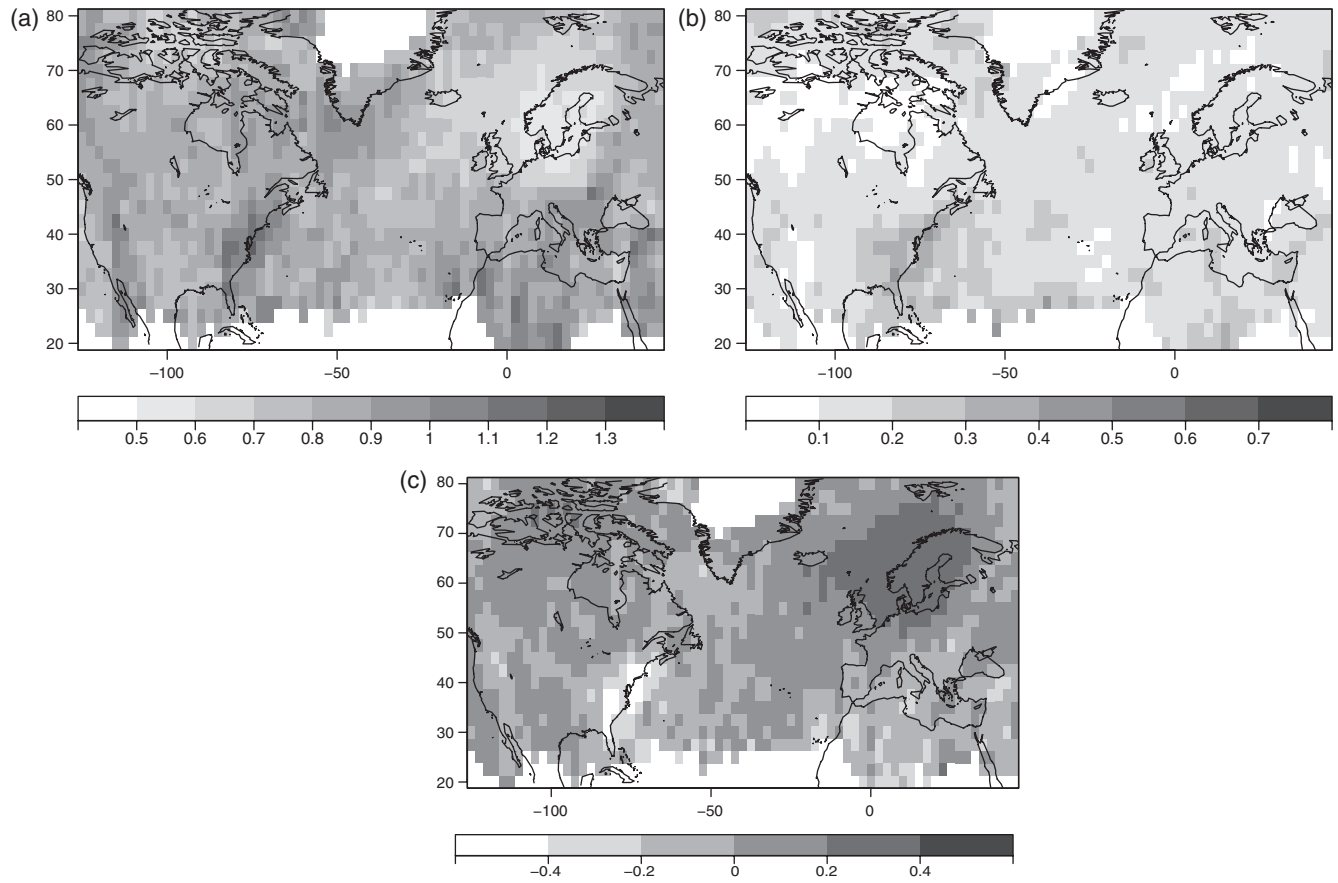

Figure 3. [Models for the variance of the aggregate risk.] Fraction of variance in s accounted for by (a) counts V_n/s_s^2, (b) cyclone intensities V_y/s_s^2 and (c) covariance between the frequency and intensity V_c/s_s^2. Stippling indicates negative values for the covariance.

The sample mean aggregate risk for the six-month winter, $\bar{s}$, and its variance, s_s^2, show a broadly similar pattern to the sample mean and variance of the cyclone counts (Figure 2(e) and (f)). This suggests that regional variation in the mean and variance of the aggregate loss might be largely accounted for by regional variation in cyclone counts. To quantify sources of variation in the aggregate risk, the sample variance of s is expressed in terms of y, as in Eq. (2), as $s_s^2 = V_n + V_y + V_c$, where

$$\begin{aligned} V_n &= s_n^2 \bar{y}^2, \\ V_y &= s_y^2 \bar{n}^2, \\ V_c &= \mathrm{cov}(n^2, y^2) - \mathrm{cov}(n, y)^2 - 2\mathrm{cov}(n, y)\bar{y}\bar{n} \end{aligned} \tag{3}$$

and cov(.) is the sample covariance between n and y (see Appendix for details). The terms V_n, V_y are non-negative, as the sample mean and variance of the counts and vorticity are non-negative. V_c can be negative if there is negative covariance between n and y. From Eqs (2) and (3), positive covariance will increase the variance of the aggregate loss (both sample and population variance); conversely, negative covariance results in lower s_s^2 and var[S]. The component due to variance in counts, V_n, accounts for a large proportion (50–80%) of the variance in the aggregate loss of extratropical cyclones over the North Atlantic storm track (see Figure 3(a)). Over the Gulf Stream, which is the primary region of cyclogenesis for the storm track, $V_n > s_s^2$ (therefore $V_c < 0$); over North Western Europe, V_n accounts for less than half of s_s^2. The variance component due to variance in intensity, V_y (Figure 3(b)), accounts for less of the variance in s than V_n; however, it still makes a significant contribution over the Gulf Stream. The variance component due to covariance between counts and intensity, V_c (Figure 3(c)), accounts for the least of the variance in s along much of the storm tracks, but is non-negligible and positive (negative) over the cyclolysis (cyclogenesis) regions for the storm tracks. Including the covariance between frequency and intensity is thus necessary for accurate modelling of the variance in the aggregate risk of extratropical cyclones in these regions.

4. Understanding the frequency–intensity dependence and its impact on aggregate risk

It is of interest to diagnose the magnitude and extent of correlation between the frequency and intensity further. In this section, the correlation between frequency and intensity is quantified for both original and detrended time series of counts and sample mean vorticity. A collective risk model is then proposed to investigate the impact of various modelling assumptions on the aggregate risk distribution.

4.1. *Sample correlation*

Figure 4 shows a map of the (Pearson's) sample correlation r between n and y. Positive correlation between the frequency and mean intensity of extratropical cyclones along the North Atlantic storm track can be seen over Scandinavia, Northern Germany and the Benelux countries ($r = 0.2 - 0.6$), as well as negative correlation over the Gulf Stream ($r = -0.3$).

Previous studies have shown that there are increasing trends in intense cyclone counts for the NCEP–NCAR reanalysis between 1950 and 2003 (e.g. (e.g. Mailier *et al.*, 2006; Vitolo *et al.*, 2009). The time series of n and y at each grid point was detrended using a first-order differencing method to assess whether the observed correlation was due to trends in both the counts and the sample local mean vorticity. Here, we define Δn and Δy as

$$\begin{aligned} \Delta y_t &= y_t - y_{t-1}, \\ \Delta n_t &= n_t - n_{t-1}, \end{aligned}$$

where t is the extended winter. Figure 4(b) shows the map of the correlation between Δn and Δy. For the North Atlantic storm

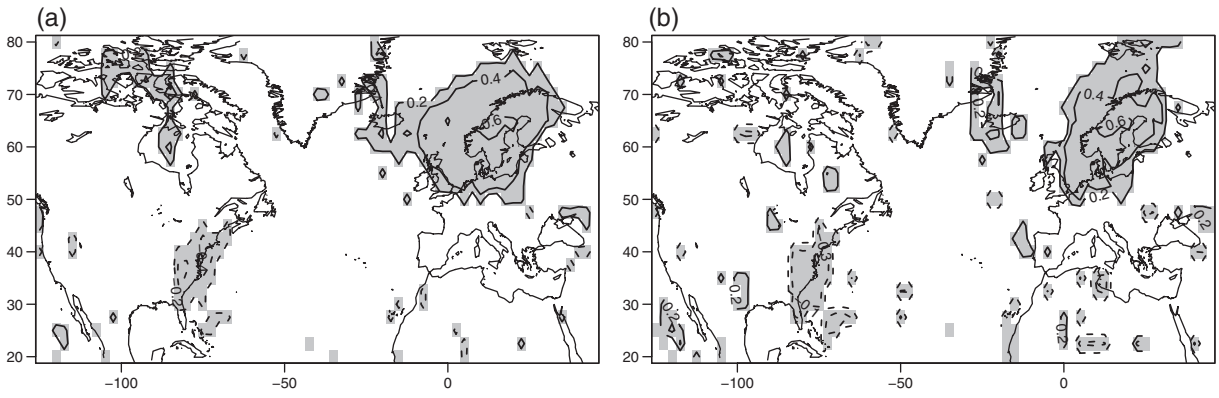

Figure 4. Map of the correlation between (a) n and y and (b) $\Delta n, \Delta y$ that is significant at the 5% level determined using the *cor.test* function in R. Solid contours denote positive correlation and dashed negative.

track, the magnitude and sign of the correlation between Δn and Δy are roughly equal to the correlation between n, y. The statistical significance of the correlation was assessed using the *cor.test* function in R and values of $\text{cor}(n, y)$ and $\text{cor}(\Delta n, \Delta y)$ that were significant at the 5% level are shown in Figure 4(a) and (b). The positive correlation over northern Europe and negative correlation over the Gulf Stream can both be seen to be statistically significant at the 5% level. From this, we can infer that the correlation between frequency and intensity of Northern European extratropical cyclones is not primarily due to trends in the data.

The sensitivity of the sample correlation to barrier width and cyclone intensity was considered briefly. Use of the $\pm 10^\circ$ barrier results in convergence of the meridians. Using a larger barrier of $\pm 20^\circ$ (not shown) results in an extension of the region of positive correlation further north above Scandinavia, but otherwise the map of the sample correlation is unchanged. The sample correlation statistic for the subset of the 50% most intense events was also investigated (not shown). The location and magnitude of the positive correlation over Scandinavia remains robust, while the negative correlation over the Gulf Stream largely disappears. This suggests the negative correlation is a feature of the weaker systems.

4.2. *Covariance between frequency and intensity*

Three parametrizations of a collective risk model are proposed here for the mean and variance of S (see Appendix for detailed derivations). The purpose of these models is to test assumptions such as that N and X are independent and X_i and X_j independent for $i \neq j$. The first parametrization, M_1, assumes there is linear dependence between N and X and only allows for covariance between consecutive cyclones. Covariance is considered between consecutive cyclones, as there may be some dependence due to secondary cyclogenesis; however, there is no reason to assume that non-neighbouring cyclones will be related. The first model assumes that

$$\begin{aligned} \mu_X|N &= \beta_0 + \beta_1 N, \\ \sigma_{XX}|N &= \begin{cases} \sigma_X^2 & \text{for} \quad i = j, \\ \rho\sigma_X^2 & \text{for} \quad i = j \pm 1, \\ 0 & \text{otherwise}, \end{cases} \end{aligned} \tag{4}$$

where ρ, σ_{XX} are the correlation and covariance between consecutive cyclone intensities, respectively. The mean and variance of S can then be shown to be given by

$$\begin{aligned} \mu_S &= \beta_0\mu_N + \beta_1(\sigma_N^2 + \mu_N^2), \\ \sigma_S^2 &= \sigma_X^2\mu_N + 2(\mu_N - 1)\rho\sigma_X^2 + \beta_0^2\sigma_N^2 + \beta_1^2\sigma_N^2 \\ &\quad + 2\beta_0\beta_1(\mu_{N^3} - \mu_N\mu_{N^2}) \end{aligned} \tag{5}$$

(see Appendix). Sample estimates for σ_X^2 (s_x^2), ρ ($\text{cor}(x_i, x_j)$) were calculated from the dataset at each grid point, along with maximum-likelihood estimates and standard errors for $\hat{\beta}_0, \hat{\beta}_1$, which were calculated using the *lm* function in R (not shown). Figure 5 shows the modelled variance σ_S^2 of the aggregate risk as well as the ratio of the modelled variance to the sample variance (σ_S^2/s_s^2). From Figure 5(a) and (b), σ_S^2 can be seen to provide a reasonable approximation to the sample variance s_s^2, as it is within $\pm 5\%$ for most grid points.

For the second model parametrization, M_2, X and N are assumed independent and Eq. (4) becomes $E[X_i] = \hat{\beta}_0 = \bar{x}$. Figure 5(c) and (d) shows that σ_S^2 underestimates s_s^2 by between 10 and 50% over the storm tracks, with the greatest discrepancy over Northern Europe. For regions of cyclogensis over the Gulf Stream, σ_S^2 is greater than the sample variance s_s^2 by up to 50% (see Figure 5(c) and (d)).

For the third model parametrization, M_3, X and N are again assumed to be linearly related but X_i, X_j are now assumed independent ($\rho = 0$). The modelled variance σ_S^2 (Figure 5(e) and (f)) provides a reasonable approximation for s_s^2, although there is some underestimation to the east of Scandinavia. The collective risk model is able to account for variance in the aggregate risk S, under suitable modelling assumptions. When X and N are assumed independent, the model underestimates the variance of S over the exit of the storm track and overestimates the variance over the Gulf Stream. Assuming independence between the intensities of consecutive cyclones does not affect the modelled variance significantly.

5. Can climate modes explain frequency–intensity dependence?

This section investigates whether the correlation between frequency and intensity could be due to joint forcing by underlying large-scale flow patterns (see Figure 6). To test this hypothesis, winter cyclone counts and sample local mean vorticity are both regressed on the same set of climate indices as explanatory variables. Similar approaches have been successful in previous studies for explaining the clustering of extratropical cyclones (Mailier *et al.*, 2006; Vitolo *et al.*, 2009).

5.1. *Large-scale flow patterns*

Barnston and Livezey (1987) identified ten teleconnection patterns that describe the state of the large-scale flow for the Northern Hemisphere. Monthly indices for these teleconnection patterns between 1950 and 2003 were obtained from the Climate Prediction Center.[§] The indices were calculated using rotated principal component analysis applied to monthly mean 700 mb

[§]http://www.cpc.ncep.noaa.gov/data/teledoc/telecontents.shtml

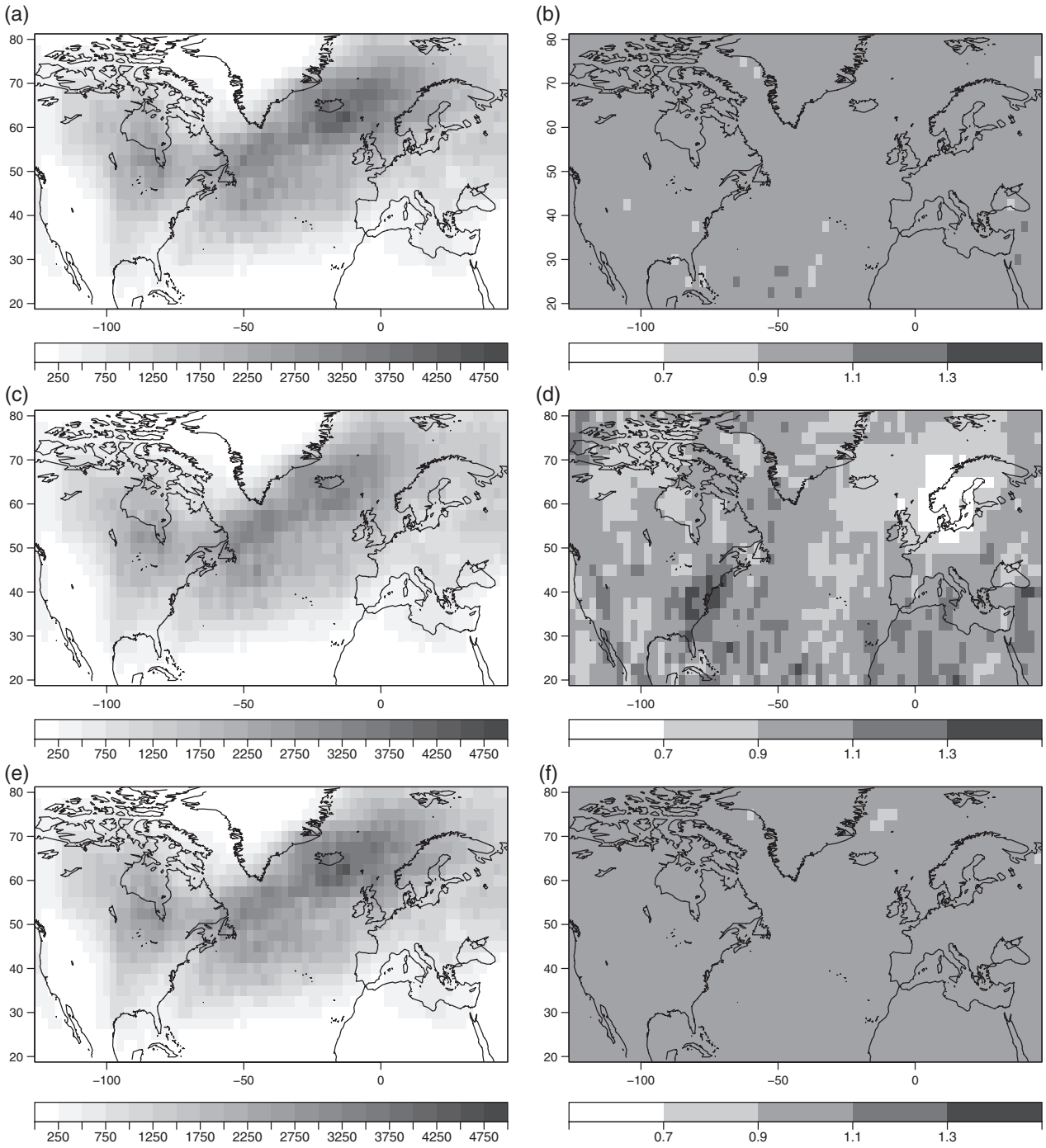

Figure 5. (a,c,e) Modelled variances σ_S^2 and (b,d,f) the ratio of the modelled variance to the sample variance σ_S^2/s_s^2 . (a,b) M_1, (c,d) M_2 and (e,f) M_3.

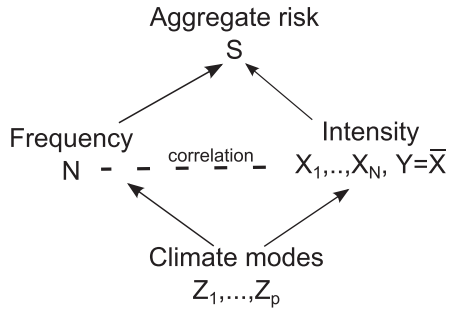

Figure 6. Schematic showing the suggested relationship between large-scale flow patterns, frequency and intensity and the aggregate risk.

geopotential height anomalies between January 1950 and July 2003, then for every month, ten leading orthogonal functions (EOFs) are selected and the amplitudes are standardized to zero mean and unit variance. The teleconnection indices are mutually uncorrelated by definition, making them useful as a basis for explanatory variables in regression models. Given the results of (Mailier *et al.*, 2006), only the first five EOFs are considered here (in order): the North Atlantic Oscillation (NAO), the East Atlantic Pattern (EAP), the Scandinavian Pattern (SCP), the East Atlantic/West Russian Pattern (EWP) and the Polar/Eurasian Pattern (POL).

The NAO, the leading mode of climate variability in the Northern Hemisphere, is characterized by a meridional dipole of pressure anomalies of opposite sign located over Iceland (low) and the Azores (high). The positive phase, which corresponds to below normal pressure over Iceland, has already been linked to increased cyclone activity over the North Atlantic in previous studies (e.g. Hurrell and Van Loon, 1997; Rogers, 1997; Trigo, 2006; Pinto *et al.*, 2009). The EAP and SCP are also important modes of variability in the winter months and describe changes in pressure and in the position and speed of the North Atlantic jet stream, which can influence cyclone activity (Bueh and Nakamura, 2007; Woollings *et al.*, 2010).

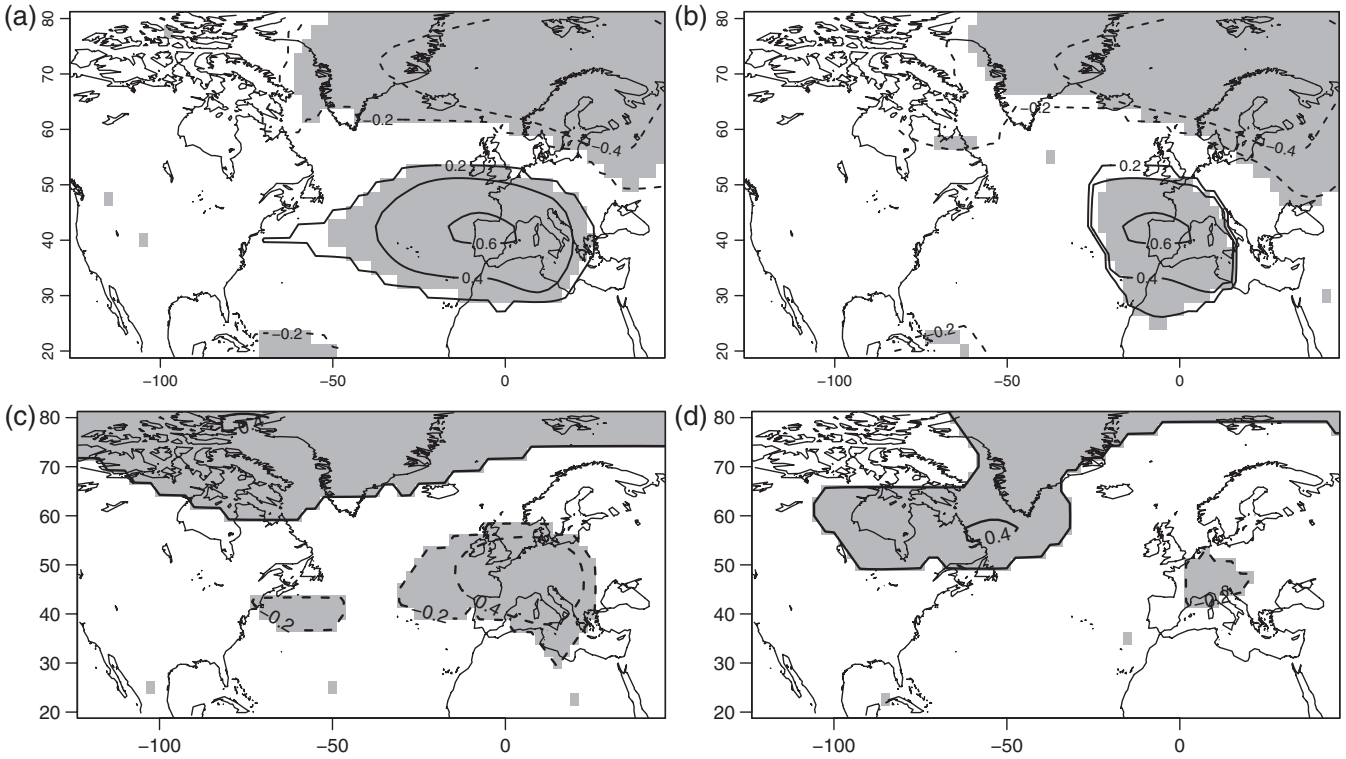

Figure 7. Plots of the correlation between the 700 mb stream function Ψ_{700} and (a) Gothenburg storm counts, (b) Gothenburg mean storm vorticity, (c) Barcelona storm counts and (d) Barcelona sample mean vorticity. Grey shading indicated that the correlation is significantly different from zero at the 5% level level according to a t test. Solid contours denote positive correlation and dashed negative.

Extratropical cyclones passing within $\pm 10^\circ$ north or south of the grid point nearest to Gothenburg (Sweden) (12.5°E, 57.5°N) were analyzed in detail, as this location exhibits the strongest positive correlation between frequency and intensity ($r = 0.47$). Cyclones passing the grid point closest to Barcelona (Spain) (2.5°E, 40°N) were also investigated, as this is a location that has low negative correlation between n and y ($r = -0.10$). Correlation maps of n, y and the 700 mb stream function were used to identify possible teleconnection patterns driving both the frequency and mean intensity of extratropical cyclones. The 700 mb stream function was chosen, as it had been used in a previous study investigating the relation between large-scale flow and extratropical cyclone activity in the same region (Bueh and Nakamura, 2007).

Correlation maps for n and y with Ψ_{700} at Gothenburg (Figure 7(a) and (b)) show a broadly similar pattern, which shows a strong resemblance to the SCP with a centre of action over Scandinavia and another of opposite sign over western Europe. The correlation of $\bar{\Psi}_{700}$ and n for Barcelona shows a centre of action centred over central Europe, with two other centres: one of opposite sign over west Russia/Kazakhstan and another of the same sign located over the Gulf Stream (Figure 7(c)). The map of the correlation between the mean intensity y and Ψ_{700} also shows a tripole pattern, except that the centre of action over Central Europe is now the weakest of the three and the location of the other two centres has been shifted northwards (Figure 7(d)). These figures suggest that there may be different physical mechanisms for the steering and intensification of cyclones near Barcelona.

5.2. *Regression modelling of frequency and intensity*

Regression models were developed for the frequency N and mean intensity Y, to assess the association with large-scale flow patterns formally. The regression models for N and Y used teleconnection patterns considered to be particularly relevant for the North Atlantic region as explanatory variables. As well as the three North Atlantic teleconnection patterns discussed above, there are the East Atlantic/West Russian (EWP) pattern and the Polar/Eurasian (POL) pattern active in the region for some winter months.

The occurrence of natural hazards is often modelled using a Poisson distribution (e.g. Katz, 2002; Mailier *et al.*, 2006). The winter cyclone counts N for Gothenburg and Barcelona were modelled as Poisson-distributed with rate parameter λ_n (see e.g. Aitkin *et al.* (2009) for more on Poisson regression in R). The mean number of cyclone counts was related to the winter means of the teleconnection patterns using the following generalized linear model (GLM):

$$N \sim \text{Poisson}(\lambda_n),$$

$$\log(\lambda_{n,t}) = \beta_0 + \sum_{k=1}^{6} \beta_k z_{k,t}$$

(see e.g. Cameron and Trivedi, 2013, section 2.3). Here $k = 1, \ldots, 6$, $t = 1, \ldots, 53$ is the year and $z_{2,t}, \ldots, z_{6,t}$ are the values of the extended winter means of the teleconnection indices for the North Atlantic in year t. The Polar/Eurasian pattern $z_{6,t}$ is inactive during October, November and March and is set to 0 for these months. The coefficient β_1 accounts for any linear time trend and $\beta_2, .. \beta_6$ are the dependences of the cyclone counts on the teleconnection patterns.

Following Vitolo *et al.* (2009), a Lagrange multiplier test is used to assess formally whether there is overdispersion/underdispersion not accounted for by the Poisson regression. This is done by testing for overdispersion against the Katz system, where the test statistic is

$$TLM = 0.5 \sum_{i=1}^{m} [(n_i - \mu_i)^2 - n_i] / \sqrt{0.5 \sum_{i=1}^{m} \mu_i^2}$$

(see Cameron and Trivedi, 2013, section 5.4.1). At Gothenburg there was found to be some (residual) underdispersion of counts, but it is not significant at the 5% level. From this and the residual analysis, the Poisson GLM is concluded to be an appropriate model for the winter cyclone counts.

Table 1. The regression coefficient estimates in the Poisson regression of cyclone counts over Gothenburg and Barcelona.

Indices	z_k	Gothenburg $\hat{\beta}_k$	Barcelona $\hat{\beta}_k$
Time	z_1	0.17 (0.14)	−0.23(0.19)
NAO	z_2	0.09 (0.06)	**−0.20** (0.09)
EAP	z_3	0.02 (0.05)	0.11 (0.07)
SCP	z_4	**−0.19** (0.06)	−0.04 (0.09)
EWP	z_5	0.03 (0.08)	−0.09 (0.11)
POL	z_6	−0.03 (0.08)	−0.21 (0.11)

Standard errors are in brackets, estimators with $p \leq 0.05$ are in bold.

Table 2. The regression coefficient estimates in the linear regression of cyclone sample local mean vorticity over Gothenburg and Barcelona.

Indices	z_k	Gothenburg $\hat{\alpha_k}$	Barcelona $\hat{\alpha_k}$
Time	z_1	**0.91** (0.29)	0.04 (0.38)
NAO	z_2	−0.12 (0.29)	0.08 (0.17)
EAP	z_3	−0.04 (0.10)	−0.23 (0.14)
SCP	z_4	**−0.58** (0.14)	0.18 (0.18)
EWP	z_5	0.09 (0.17)	0.22 (0.22)
POL	z_6	−0.10 (0.17)	−0.39 (0.22)

Standard errors are in brackets, estimators with $p \leq 0.05$ are in bold.

Maximum-likelihood estimates for the coefficients ($\hat{\beta}_k$) for the winter count models for Gothenburg and Barcelona are given in Table 1. For the grid point closest to Gothenburg, only the SCP showed a significant (according to a t-test at the 5% level) relationship with the winter cyclone counts. The SCP is negatively associated with the number of cyclones passing near Gothenburg. For extratropical cyclones passing near Barcelona, only the NAO shows a significant (negative) relationship with counts. These findings are consistent with those of Mailier *et al.* (2006) and Vitolo *et al.* (2009), where the SCP slope estimate was significant over most of Scandinavia, including the Gothenburg grid cell.

Normal linear regression was found to be suitable for modelling winter sample local mean vorticity Y, with the modelled intensity regressed against the same teleconnection indices as the modelled counts. The extended winter sample local mean vorticity is then

$$Y \sim N(\mu_y, \sigma),$$
$$\mu_{y,t} = \alpha_0 + \sum_{k=1}^{6} \alpha_k z_{k,t}.$$

The $z_{k,t}$ is the same as for the Poisson model and the regression coefficient estimates α_k have the same interpretations as above, except that they are (linearly) related to winter sample local mean vorticity instead of cyclone counts.

Maximum-likelihood estimates for the regression coefficients for Gothenburg and Barcelona sample mean vorticity ($\hat{\alpha_k}$) are given in Table 2. The estimate for the time trend coefficient $\hat{\alpha_1}$ is highly significant over Gothenburg, suggesting non-stationarity in the winter mean intensity. This is consistent with Vitolo *et al.* (2009), where non-stationarity was found for the counts of intense cyclones over the same region, but not for all cyclones. In Vitolo *et al.* (2009) it was suggested that the increase in the rate of intense cyclones could be due to either climatic change or inhomogeneities in the reanalysis dataset. The SCP coefficient ($\hat{\alpha_4}$) is also highly significant for Gothenburg winter sample mean vorticity, suggesting that this may be a driver of cyclone intensity. The model of Gothenburg sample mean vorticity has an R^2 value of 0.49, meaning that just under half the variance in sample local mean vorticity is explained by the model. For Barcelona, none of the teleconnection indices is significant at the 5% level, although the EAP and POL are significant at the 10% level. The Barcelona model has a lower R^2 value of 0.22, suggesting large-scale flow patterns are of less use in explaining winter mean intensity over this region.

5.3. *Modelled covariance*

The modelled covariance between $\hat{N}$ and $\hat{Y}$ for Gothenburg can be expressed as

$$\begin{aligned}\mathrm{cov}(\hat{N}, \hat{Y}) &= \mathrm{cov}(\alpha_0 + \alpha_1 z_1 + ...\alpha_6 z_6, \mathrm{e}^{\beta_0 + \beta_1 z_1 + ...\beta_6 k z_6}) \\ &= \mathrm{cov}(\alpha_1 z_1, \mathrm{e}^{\beta_1 z_1}) + \mathrm{cov}(\alpha_2 z_2, \mathrm{e}^{\beta_2 z_2}) + \mathrm{cov}(\alpha_3 z_3, \mathrm{e}^{\beta_3 z_3}) \\ &+ \mathrm{cov}(\alpha_4 z_4, \mathrm{e}^{\beta_4 z_4}) + \mathrm{cov}(\alpha_5 z_5, \mathrm{e}^{\beta_5 z_5}) + \mathrm{cov}(\alpha_6 z_6, \mathrm{e}^{\beta_6 z_6}),\end{aligned} \quad (6)$$

since the teleconnection indices are uncorrelated by definition and so $\mathrm{cov}(z_i, z_j) = 0$ when $i \neq j$. From Eq. (6) and the modelled standard deviations $\sigma_{\hat{N}}, \sigma_{\hat{Y}}$ the modelled correlation can be estimated for Gothenburg, $\mathrm{cor}(\hat{N}, \hat{Y}) = 0.32$ (compared with the observed correlation $\mathrm{cor}(n, y) = 0.48$). The regression models using teleconnection indices as explanatory variables account for two thirds of the correlation over Gothenburg. Using the same method for Barcelona, the modelled correlation is $\mathrm{cor}(\hat{N}, \hat{Y}) = -0.02$. Regression models using teleconnection indices as explanatory variables are thus suitable for reproducing the positive correlation between N and Y over northern Europe. For cyclones passing near Barcelona, teleconnection indices are possible drivers for the cyclone counts but not for the sample mean vorticity.

6. Regression models for all grid points

The analysis conducted at Gothenburg and Barcelona was repeated for all Northern Hemisphere grid points. The regression coefficients for the linear trend term, the NAO, SCP and EAP were significant for the models for N and Y over much of the North Atlantic and Europe. Reduced models with only these four explanatory covariates are now assessed.

The maximum-likelihood estimates of the North Atlantic regression parameters for cyclone counts and sample local mean vorticity, $\hat{\beta}_k$ and $\hat{\alpha_k}$, $k = 1, .., 4$ are shown in Figures 8 and 9 respectively. Statistical significance was determined with a t test at the 5% level. There is a clear relationship between large-scale flow patterns and both winter cyclone counts and winter sample local mean vorticity (Figures 8 and 9). The NAO parameter for counts is statistically significant over much of the North Atlantic (Figure 9(b)). The positive phase of the NAO is associated with an increase in extratropical cyclones across Canada, Greenland and Iceland as well as north Great Britain, as well as with a decrease in cyclones over the northwest coast of Africa. Although the NAO appears to be the single greatest driver in cyclone counts of the three teleconnection indices considered here, it is not significant for the modelled winter cyclone counts over the region of Europe (Scandinavia, North Germany, Great Britain, Benelux), where the positive correlation was observed (Figure 4(a)). The NAO parameter for sample local mean vorticity is significant over Iceland and most of the Norwegian sea. There appear to be very few grid points where the NAO parameter is significant for *both* frequency and intensity. From Figure 8(c), the SCP coefficient for counts is significant over a region extending from the east coast of Greenland over Scandinavia and into eastern Europe. The SCP coefficient estimate for sample local mean vorticity (Figure 9(c)) is significant over Scandinavia, north Germany and the Benelux countries. From these plots, it would seem likely that, as with Gothenburg, the SCP coefficients account for much of the correlation because of their importance for explaining both counts and mean intensity in many locations.

The EAP coefficient is significant for cyclone counts over the east coast of the United States across the Atlantic up to the Iberian Peninsula (Figure 8(d)) . The EAP coefficient is also significant for sample local mean vorticity over some grid points in the eastern United States and to the southeast of Greenland (Figure 9(d)). There are few grid points where the EAP coefficient is significant

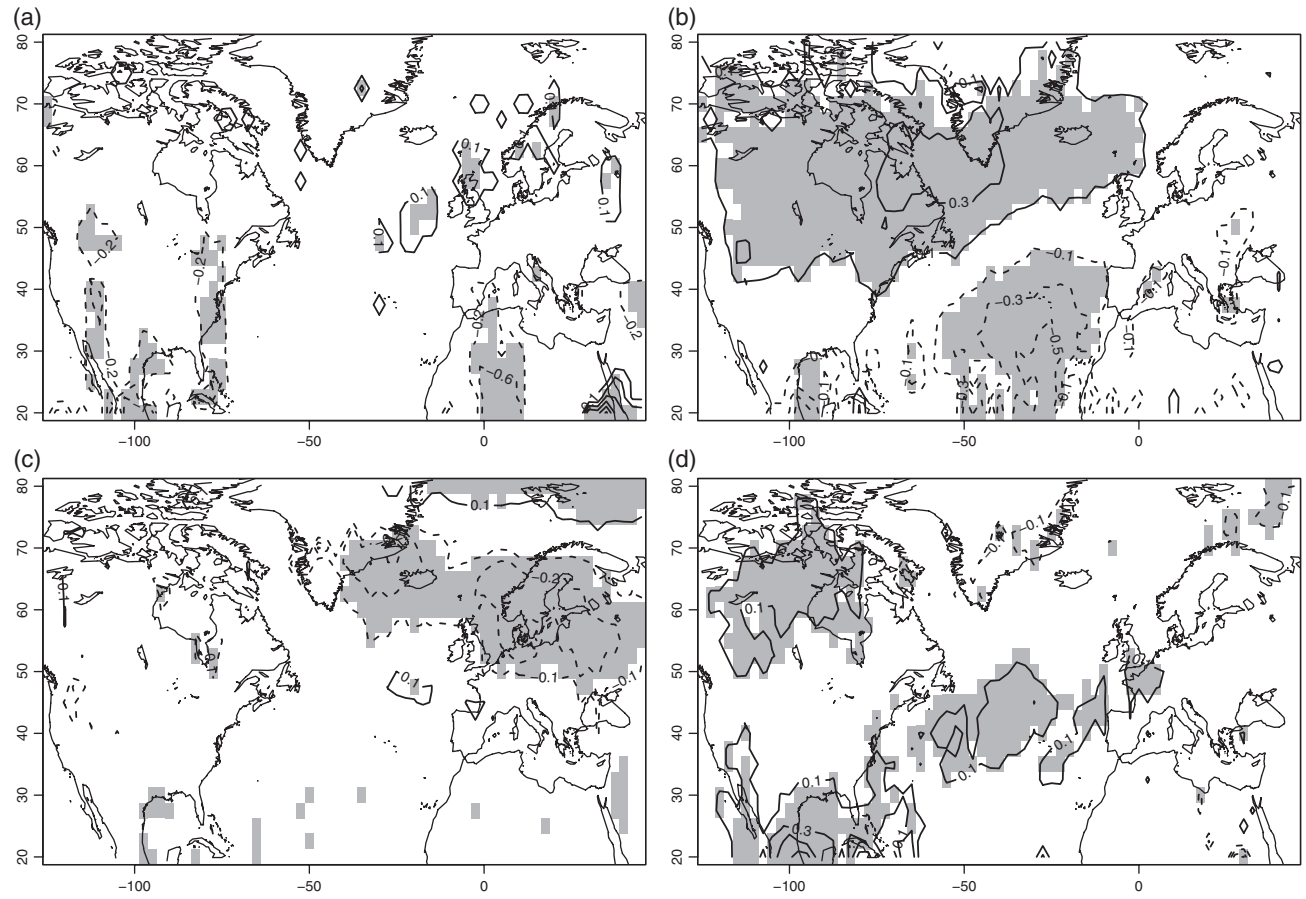

Figure 8. Slope estimates from a Poisson regression of storm counts, on (a) a linear time trend, (b) the North Atlantic Oscillation, (c) the Scandinavian pattern and (d) the East Atlantic Pattern. Solid (dashed) lines indicate positive (negative) values and grey shading means the coefficient is significantly different from zero at the 5% level level, according to a *t* test.

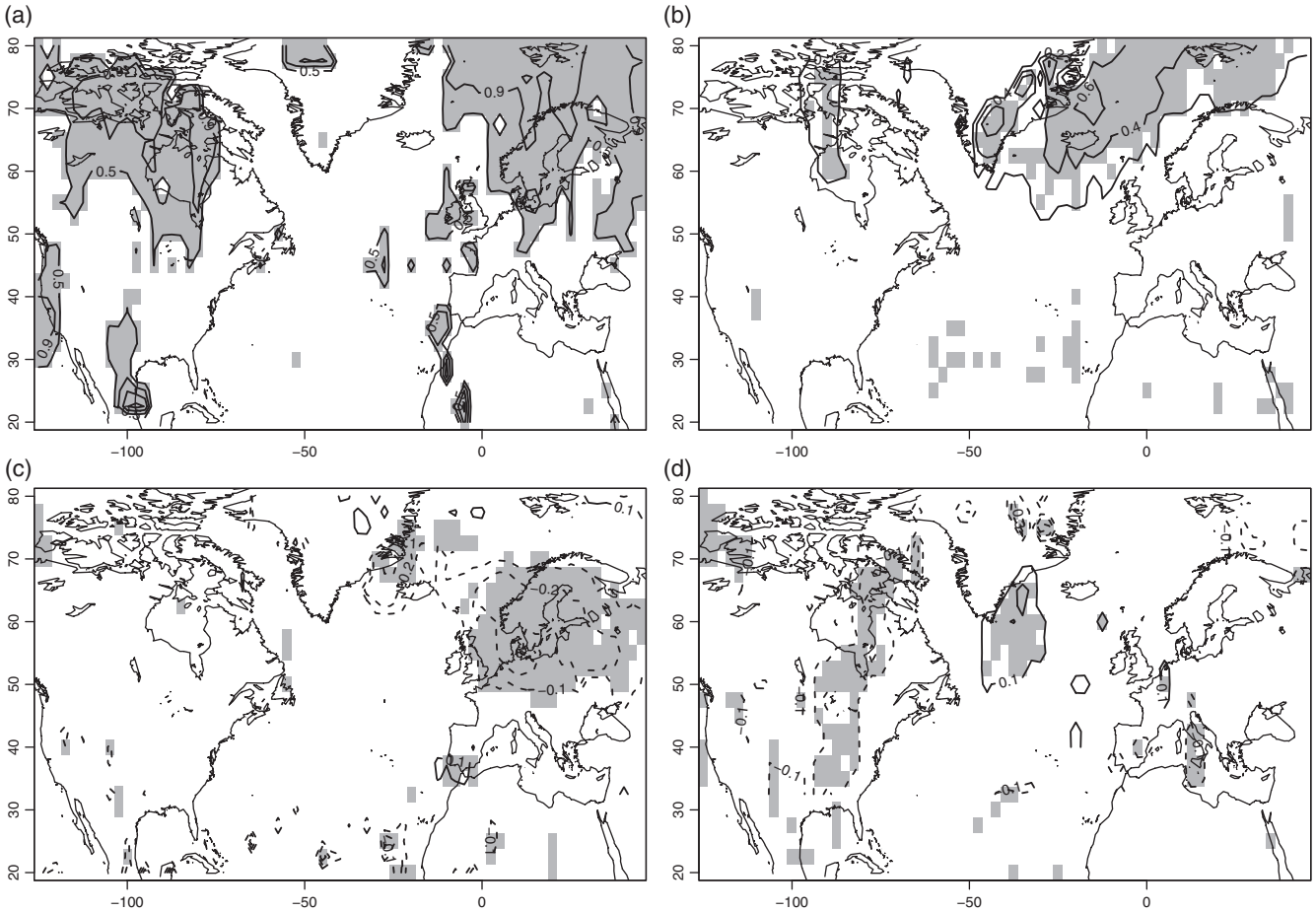

Figure 9. Slope estimates from a multiple linear regression of sample mean vorticity on (a) a linear time trend, (b) the North Atlantic Oscillation, (c) the Scandinavian pattern and (d) the East Atlantic Pattern. Solid (dashed) lines indicate positive (negative) values and grey shading means the coefficient is significantly different from zero at the 5% level level, according to a *t* test.

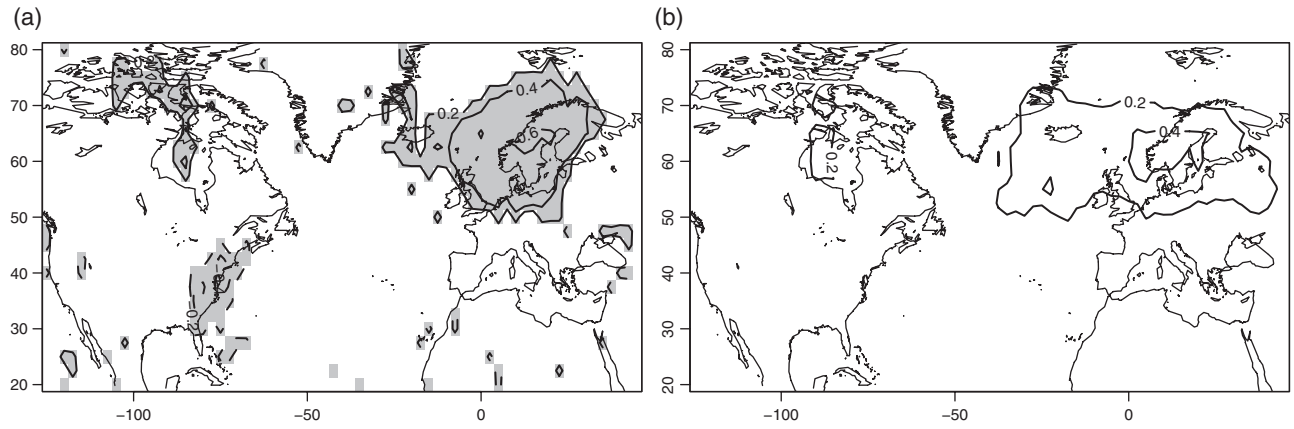

Figure 10. Plots of (a) the sample correlation and (b) the modelled correlation between cyclone counts n and sample mean vorticity y. Grey shading indicates the correlation is significantly different from zero at the 5% level, according to a t test. Solid contours denote positive correlation and dashed negative.

for both counts and intensity. The time trend coefficient for counts is significant for part of the United States eastern seaboard and for a few grid points over and around the north of Great Britain. For sample local mean vorticity, the time trend coefficient is significant for a large region of North Europe and over Canada. This agrees with the findings in Vitolo *et al.* (2009), where a linear time trend was not found to be significant for Poisson regression of three-monthly counts over most grid points, but was found to be significant over Canada and northwestern Europe.

The coefficient estimates for the SCP are significant for both counts and mean intensity over much of the Scandinavian peninsula, as well as parts of Northern Germany and the Benelux countries. The plot of the modelled correlation (Figure 10) shows that the large-scale flow patterns account for much of the observed positive correlation for the Atlantic region.

7. Discussion of possible physical mechanisms

The Scandinavian pattern modulates both cyclone frequency and mean intensity and thereby induces a positive correlation between frequency and intensity. Possible physical mechanisms for how the Scandinavian pattern interacts with extratropical cyclones are discussed here. The negative correlation observed over the Gulf Stream is also briefly considered.

7.1. Positive correlation

In the previous section, it was shown that negative phases of the Scandinavian pattern are associated with increased cyclone activity; more occurrences with higher mean intensity. It is important to distinguish between cause and effect, as increased cyclone activity may also result in persistent negative SCP index values. The potential for synoptic-scale activity, such as cyclones, to influence the state of the background flow has been discussed in the literature, such as in Pinto *et al.* (2009), where it explains that cyclones themselves may play a major role in steering the phase of the NAO. However, in Whitaker and Sardeshmukh (1998) it was shown that, while transient eddies/cyclones can affect the background upper tropospheric circulation, the latter is more important in initiating eddy formation and controlling intensification.

Four key environmental factors that control cyclone intensification were considered in Pinto *et al.* (2009): latent energy (equivalent potential energy 850 hPa), upper-air baroclinicity, horizontal divergence and jet-stream strength. The growth of extreme cyclones was shown to be related to these four explanatory variables, with the jet-stream location and velocity in particular showing a clear connection to extreme cyclone intensification. The major (i.e. NAO, EAP, SCP) extratropical teleconnections essentially describe jet-stream variability over the ocean basins (Woollings *et al.*, 2010).

In Raible (2007), the occurrence of extreme intensified cyclones in Northern Europe is linked to a rotated NAO-like pattern, which corresponds to the SCP as identified here and discussed in section 5.1. In Hanley and Caballero (2012), it was also shown that intense European extratropical cyclones occurred during an eastward-shifted NAO-like pattern, which is again qualitatively similar to a negative phase of the Scandinavian pattern. The large-scale low-pressure system located over the Scandinavian peninsula, associated with negative values of the SCP index, helps steer extratropical cyclones into Northern Europe, as well as generating an intense baroclinic jet streak that acts to intensify cyclones. In particular, a case study of extreme storm *Daria* was conducted that showed that the background atmospheric conditions *preceded Daria*'s birth (Hanley and Caballero, 2012) .

Most of the studies cited above have investigated the link between environmental factors and cyclone clustering over synoptic time-scales. Synoptic variability over the North Atlantic and Europe is related to the NAO and other teleconnection patterns, which in turn has been related to the occurrence and development of cyclones over synoptic time-scales (Pinto *et al.*, 2009). However, this study has considered aggregate cyclone activity over a longer six-month extended winter period. The same arguments put forward for linking teleconnection patterns and extratropical cyclone activity for shorter time periods remain valid for the six-month aggregated period. In particular, the winter mean NAO has been linked to interannual variability in the mid-tropospheric baroclinicity (Baldwin *et al.*, 1994). The baroclinicity in the mid-troposphere is related to surface temperature gradients, which in turn influence cyclone activity (Raible, 2007).

The relation between the Scandinavian pattern and its climatic impact, as well as possible forcing mechanisms, is discussed in Bueh and Nakamura (2007). For negative phases of the SCP, 200 mb zonal wind anomalies are observed over Northern Europe over the same region in which positive correlation is observed (see figure 3 of Bueh and Nakamura, 2007), as well as increased baroclinicity over the same area. It was shown in Bueh and Nakamura (2007) that there is positive feedback over the exit region of the North Atlantic storm track between the Scandinavian pattern and passing cyclones. This positive feedback between extratropical cyclones and the background atmospheric flow is a possible mechanism for the frequency–intensity dependence found here, as well as the observed clustering of intense cyclones shown in Vitolo *et al.* (2009); favourable environmental conditions result in increased cyclone activity through enhanced steering and intensification, which in turn help to maintain these conditions.

This work is of particular relevance to the insurance industry. Whilst many catastrophe reinsurance contracts begin on 1 January, others begin at different dates, for example from 1 April or 1 July. Therefore a reinsurance contract may cover two halves of different consecutive winter seasons (1 January renewal)

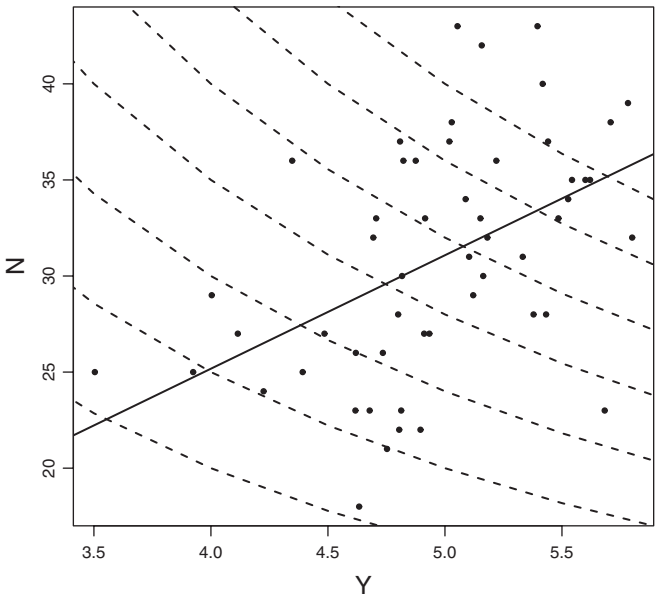

Figure 11. Plot of sample mean vorticity Y against storms counts N for extratropical cyclones passing near Gothenburg. Contours of S have been added for $S = 80, 100, 120, 140, 160, 180, 200$.

or one whole winter season. If frequency intensity dependence results in increased financial risk from extratropical cyclones for the entire winter season, there will also be an impact, albeit smaller, from the combination of two independent half-seasons.

7.2. *Negative correlation*

The negative correlation discovered over the Gulf Stream is also possibly due to some interaction between the background atmospheric flow and extratropical cyclones. However, none of the regression coefficients from either the North Atlantic or the North Pacific sample local mean vorticity models are significant over the Gulf Stream. One possible mechanism is the velocity and position of the North Atlantic subtropical and/or eddy-driven jet stream. In Pinto *et al.* (2009), factors contributing to the development of extreme North Atlantic cyclones was considered. It was shown that during strongly positive phases of the NAO the jet stream over North America is enhanced, resulting in increased cyclogenesis and more extreme storms over the North Atlantic. However, extratropical cyclones originating from the West Atlantic/North American east coast typically develop slowly, not reaching maximum intensification until further East into the Atlantic (Dacre and Gray, 2009). In Pinto *et al.* (2009), it can be seen that during strongly negative NAO phases, although there are fewer extreme cyclones, they reach their point of maximum intensification closer to the eastern United States.

8. Extremes of aggregate risk

Extremes in the aggregate risk are due to either an above average number of occurrences or the occurrence of one or more high-intensity events, or a combination of both (see Figure 11). As discussed in section 2, analytic results for the distribution of S, F_S, are generally not available except under certain restrictive conditions. Uncertainty would be large when trying to estimate the distribution of extremes through simulation, so instead bootstrapped confidence intervals and Cantelli bounds are used to investigate upper limits on the quantiles of the aggregate risk distribution.

8.1. *Bootstrap confidence intervals*

Bootstrap confidence intervals can be constructed to estimate upper bounds for the return levels of aggregate risk. By assuming independence between the frequency and intensity, a block bootstrapping method can be used to construct confidence intervals for the return level at T years (and thus the exceedance probabilities $p = 1 - 1/T$) as follows.

For r in $1, \ldots, R$:

(1) construct a resampled (with replacement) time series of cyclone counts $n^*_{1,r}, \ldots, n^*_{m,r}$;
(2) construct a resampled (with replacement) time series of cyclone sample local mean vorticity $y^*_{1,r}, \ldots, y^*_{m,r}$;
(3) calculate the corresponding time series of aggregate losses $s^*_{1,r}, \ldots, s^*_{m,r}$ for each r from the resampled counts and sample local mean vorticity; and
(4) calculate the new resampled return levels; $q^*_{p,r}(s)$. Here, $q^*_{p,r}(s)$ is the empirical quantile estimate for the rth resampled time series of aggregate losses s.

Then the 90% confidence intervals for the pth quantile are the 5th and 95th percentiles of the resampled $q^*_{p,r}(s)$. As n and y are assumed to be independent in this bootstrapping algorithm, if the empirical return level plot for s diverges outside the confidence intervals this would provide an indicator that the inclusion of frequency–intensity dependence is necessary to model extremes of aggregate loss.

8.2. *Cantelli bounds*

Upper bounds for return levels can be calculated from Cantelli's inequality (Royden, 1953). This states that, for a positive real random variable S with mean μ_s and variance σ^2_S,

$$\Pr(S \geq \mu_S + k\sigma_S) \leq \frac{1}{1+k^2} = \frac{1}{T}, \tag{7}$$

where $k \geq 0$ and T is the return time. Cantelli bounds can be used to consider the effect of covariance between the frequency and intensity on the aggregate loss S for exceedance probabilities beyond those that have been observed. To do this, two cases are considered: in the first, the frequency and intensity are considered independent and μ_S, s^2_S are estimated as

$$\bar{s} = \bar{n}\bar{y},$$
$$s^2_s = V_n + V_y,$$

as in section 2. In the second case, the the sample mean and variance of s are

$$\bar{s} = \bar{n}\bar{y} + \mathrm{cov}(n, y),$$
$$s^2_s = V_n + V_y + V_c,$$

which will result in increased Cantelli bounds in Eq. (7), when $\mathrm{cov}(n, y) > 0$, and reduced Cantelli bounds when $\mathrm{cov}(n, y) < 0$.

8.3. *Results*

The empirical return level plots for s at Gothenburg and Barcelona are shown in Figure 12. The bootstrap intervals assume the sample counts n and sample local mean vorticity y are independent. For Gothenburg (Figure 12(a)), this assumption is not valid and the empirical aggregate exceedance probability (AEP) curve is outside the bootstrapped intervals for the upper and lower tails, suggesting that extremes of aggregate loss (both high and low) are sensitive to frequency–intensity dependence. The Barcelona sample aggregate loss is contained within the intervals, suggesting that the small amount of negative dependence at this location does not affect the extremes significantly.

The Cantelli bounds provide a (high) upper bound for the return levels. At Gothenburg, the Cantelli bounds with and without dependence diverge with increasing return period, where

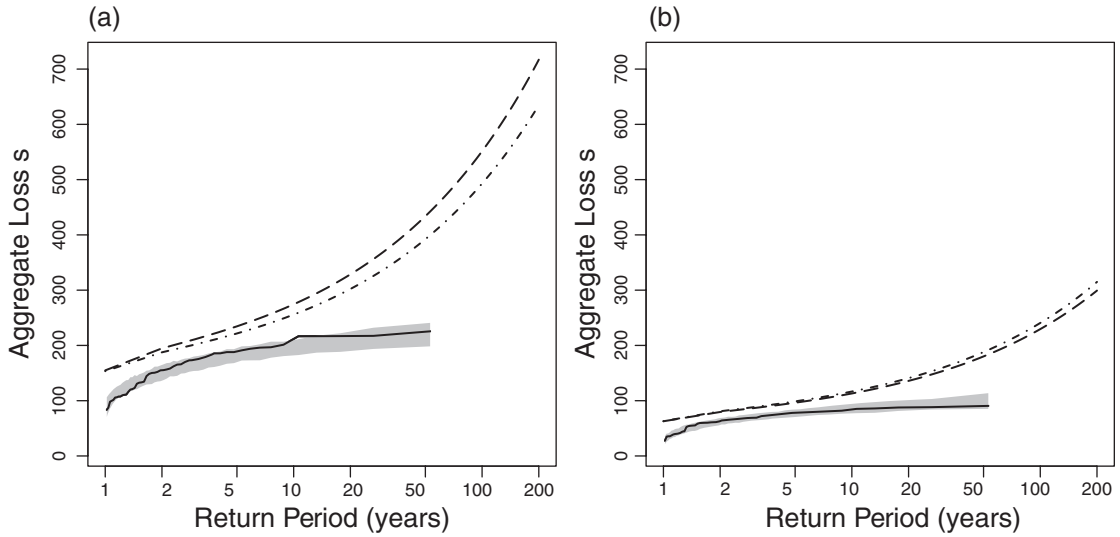

Figure 12. Empirical return level of aggregate loss for extratropical cyclones s (solid lines) with 90% bootstrap confidence intervals (grey shading) and Cantelli bounds (dashed line X, N non-i.i.d, dash–dotted line X, N i.i.d) against the return period in years at (a) Gothenburg and (b) Barcelona.

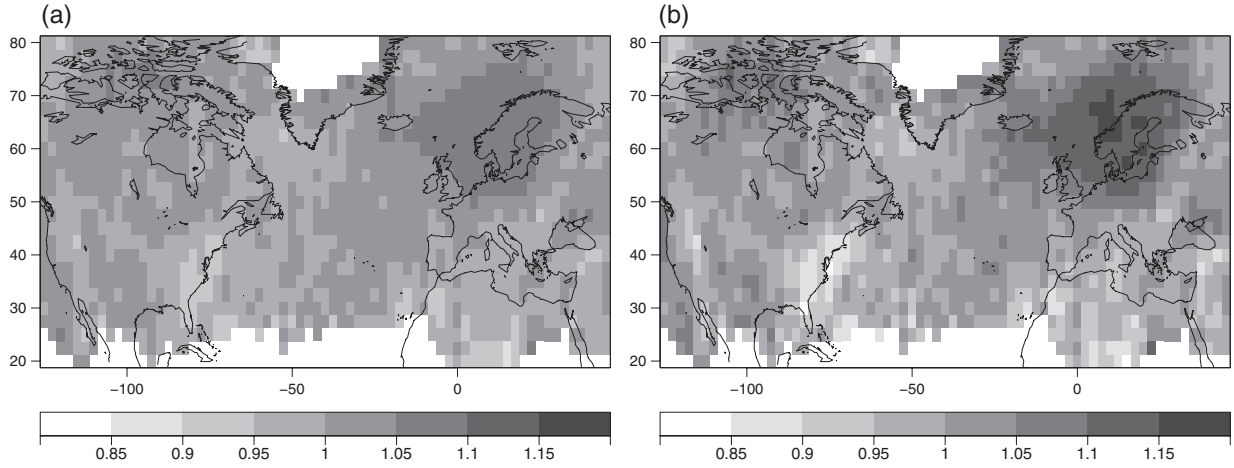

Figure 13. Plots of the ratio of the Cantelli bounds S_D/S_I for (a) the 10 year return level and (b) the 200 year return level.

the upper bound for s is greater when dependence is included (Figure 12(a)). At Barcelona, the relation is reversed: the Cantelli bound with dependence has lower return levels than the bound without dependence, although the difference between bounds is less than at Gothenburg (Figure 12(b)). As with the bootstrapped confidence intervals, this suggests that a positive dependence between frequency and intensity results in an increase in extremes of aggregate loss. Conversely, negative dependence may result in a decrease.

The percentage change in the Cantelli bounds for $T = 200$ in Eq. (7) with the inclusion of dependence was +13.0% at Gothenburg and −5.0% at Barcelona. The ratios for the 1 in 10 year return levels with/without dependence and 1 in 200 year return levels with/without dependence were calculated for all Northern Hemisphere grid points (Figure 13). Similar conclusions to those from Gothenburg and Barcelona can be drawn: locations with positive (negative) dependence show an increase (decrease) in the upper bound for return levels of aggregate risk when the dependence is included and the difference between the bounds increases with greater return periods.

9. Conclusions

This article introduces a framework for quantifying the aggregate risk of extratropical cyclones. This framework is then applied to extratropical cyclones using a database of tracks for the Northern Hemisphere (covering October–March winters from 1950–2003). Statistical models were used to investigate the sensitivity of the variance of the aggregate risk to the dependence between the frequency and intensity of cyclones as well as the dependence between successive events.

A statistically significant correlation was found between the frequency and intensity of extratropical cyclones over parts of northern Europe, including Scandinavia, Germany and Great Britain as well as the eastern end of the North Atlantic storm track. The findings for extended winter cyclone counts agreed with those of Vitolo *et al.* (2009) concerning linear trends in intense cyclones over Scandinavia and the effect of large-scale flow patterns on cyclone counts.

Joint modulation by large-scale flow patterns is shown to be responsible for generating the covariance between cyclone frequency and mean intensity. The Scandinavian pattern, in particular, is strongly negatively correlated with both counts and sample local mean vorticity over much of northern Europe. Regressing the counts and sample local mean vorticity on the Scandinavian pattern index reproduces most of the observed correlation. Other important teleconnection indices for both frequency and intensity are the North Atlantic Oscillation and the East Atlantic pattern.

Non-parametric Cantelli bounds and bootstrap confidence intervals were used to investigate the effect of frequency–intensity dependence on the extremes of the aggregate risk distribution for extratropical cyclones passing near Gothenburg and Barcelona. Positive (negative) dependence was shown to result in an increase (decrease) in the exceedance levels. Therefore any statistical model for extratropical cyclone risk that (falsely) assumes frequency–intensity independence will understimate the return periods for extreme events.

The framework presented here is relevant to other natural hazards that have been shown to cluster, e.g. floods and hurricanes (Mumby *et al.*, 2011; Villarini *et al.*, 2013). The aggregate risk for any type of meteorological event where the dependence between frequency and intensity is not properly modelled could be underestimated.

Acknowledgements

Alasdair Hunter has been supported by a NERC industrial CASE PhD award kindly supported by the Willis Research Network.

The authors gratefully acknowledge Dr Kevin Hodges for providing the storm tracks and Dr Jonty Rougier for the suggestion of using Cantelli bounds.

Appendix A: Analysis of modelling assumptions

To investigate the effect of modelling assumptions, such as N and X being independent, a collective risk model was proposed, where

$$\mu_X|N = \beta_0 + \beta_1 N,$$
$$\sigma_{XX}|N = \begin{cases} \sigma_X^2 & \text{for} \quad i = j, \\ \rho\sigma_X^2 & \text{for} \quad i = j \pm 1, \\ 0 & \text{otherwise,} \end{cases}$$

where σ_{XX} is the covariance and ρ the correlation between X_i and X_j. This gives

$$\begin{aligned} \mu_S &= E_N\left[\beta_0 N + \beta_1 N^2\right] = \beta_0\mu_N + \beta_1\left(\sigma_N^2 + \mu_N^2\right) \\ \sigma_S^2 &= E_N[N\sigma^2 + 2N(N-1)\rho\sigma^2] + \mathrm{var}_N\left(\beta_0 N + \beta_1 N^2\right) \\ &= \sigma^2\mu_N + 2\left(\mu_N - 1\right)\rho\sigma^2 \\ &\quad + \beta_0^2\sigma_N^2 + \beta_1^2\sigma_{N^2}^2 + 2\beta_0\beta_1\left(\mu_{N^3} - \mu_N\mu_{N^2}\right), \end{aligned} \tag{A1}$$

since

$$\begin{aligned} \mathrm{var}\left(\beta_0 N + \beta_1 N^2\right) &= \beta_0^2\mathrm{var}[N] \\ &\quad + \beta_1^2\mathrm{var}[N^2]^2 + 2\beta_0\beta_1\mathrm{cov}[N, N^2] \end{aligned}$$

and

$$\mathrm{cov}[N, N^2] = \mu_{N^3} + \mu_N\mu_{N^2}.$$

Sample estimators

Consider a dataset with years $t = 1, 2, \ldots, T$. Each year there are n_t events and for each event there is a severity measure $x_{1,t}, x_{2,t} \ldots x_{n_t,t}$. The estimators for the sample mean and variance of variable n are denoted $\bar{n}, s_n^2$:

$$\bar{n} = \frac{1}{T}\sum_{t=1}^{T} n_t,$$
$$s_n^2 = \frac{1}{T-1}\left(\sum_{t=1}^{T} n_t - \bar{n}\right)^2.$$

The sample mean vorticity y_t in year t is

$$y_t = \frac{1}{n_t}\sum_{i=1}^{n_t} x_{i,t},$$
$$\bar{y} = \frac{1}{T}\sum_{t=1}^{T} y_t,$$
$$s_y^2 = \frac{1}{T-1}\left(\sum_{t=1}^{T} y_t - \bar{y}\right)^2.$$

The sample estimator for the covariance between n and y is

$$\mathrm{cov}(n, y) = \frac{1}{T-1}\sum_{t=1}^{T}(n_t - \bar{n})(y_t - \bar{y}).$$

The sample aggregate risk is

$$s_t = \sum_{i=1}^{n_t} x_{i,t},$$
$$\bar{s} = \frac{1}{T}\sum_{t=1}^{T} s_t,$$
$$s_s^2 = \frac{1}{T-1}\left(\sum_{t=1}^{T} s_t - \bar{s}\right)^2.$$

References

Aitkin M, Francis B, Hinde J, Darnell R. 2009. *Statistical Modelling in R*. Oxford University Press: Oxford, UK.

Baldwin MP, Cheng X, Dunkerton TJ. 1994. Observed correlations between winter-mean tropospheric and stratospheric circulation anomalies. *Geophys. Res. Lett.* **21**: 1141–1144, doi: 10.1029/94GL01010.

Barnston A, Livezey R. 1987. Classification, seasonality and persistence of low-frequency atmospheric circulation patterns. *Mon. Weather Rev.* **115**: 1083–1126.

Blender R, Raible C, Lunkeit F. 2015. Non-exponential return time distributions for vorticity extremes explained by fractional Poisson processes. *Q. J. R. Meteorol. Soc.* **141**: 249–257.

Borch K. 1967. The theory of risk. *J. R. Stat. Soc. Ser. B: Methodol.* **29**: 432–467.

Bueh C, Nakamura H. 2007. Scandinavian pattern and its climatic impact. *Q. J. R. Meteorol. Soc.* **133**: 2117–2131.

Cameron AC, Trivedi P. 2013. *Regression Analysis of Count Data*, Vol. 53. Cambridge University Press: Cambridge, UK.

Dacre HF, Gray SL. 2009. The spatial distribution and evolution characteristics of North Atlantic cyclones. *Mon. Weather Rev.* **137**: 99–115.

Embrechts P, Klüppelberg C, Mikosch T. 1997. *Modelling Extremal Events: For Insurance and Finance*, Vol. 33. Springer: New York, NY.

Frishman F. 1971. *Statistical Distributions in Scientific Work*. Reidel: Dordrecht, Netherlands.

Hanley J, Caballero R. 2012. The role of large-scale atmospheric flow and Rossby wave breaking in the evolution of extreme windstorms over Europe. *Geophys. Res. Lett.* **39**: L21708, doi: 10.1029/2012GL053408.

Hodges KI. 1994. A general method for tracking analysis and its application to meteorological data. *Mon. Weather Rev.* **122**: 2573–2586.

Hodges KI. 1999. Adaptive constraints for feature tracking. *Mon. Weather Rev.* **127**: 1362–1373.

Hodges KI. 1995. Feature tracking on the unit-sphere. *Mon. Weather Rev.* **123**: 3458–3465.

Hodges KI, Hoskins BJ, Boyle J, Thorncroft C. 2003. A comparison of recent reanalysis datasets using objective feature tracking: Storm tracks and tropical easterly waves. *Mon. Weather Rev.* **131**: 2012–2037.

Hoskins BJ, Hodges KI. 2002. New perspectives on the Northern Hemisphere winter storm tracks. *J. Atmos. Sci.* **59**: 1041–1061.

Houston DB. 1960. Risk theory. *J. Insur.* **27**: 77–82.

Hurrell JW, Van Loon H. 1997. Decadal variations in climate associated with the north Atlantic oscillation. In *Climatic Change at High Elevation Sites*, Diaz HF, Beniston M, Bradley R. (eds.): 69–94. Springer: Netherlands.

Kalnay E, Kanamitsu M, Kistler R, Collins W, Deaven D, Gandin L, Iredell M, Saha S, White G, Woolen J, Zhu Y, Chelliah M, Ebisuzaki W, Higgens W, Janowiak J, Mo KC, Ropelewski C, Wang J, Leetma A, Reynolds R, Jenne R, Joseph D. 1996. The NCEP–NCAR 40-year reanalysis project. *Bull. Am. Meteorol. Soc.* **77**: 437–471.

Katz R. 2002. Stochastic modeling of hurricane damage. *J. Appl. Meteorol.* **41**: 754–762.

Katz RW, Parlange MB. 1998. Overdispersion phenomenon in stochastic modeling of precipitation. *J. Clim.* **11**: 591–601.

Kistler R, Collins W, Saha S, White G, Woollen J, Kalnay E, Chelliah M, Ebisuzaki W, Kanamitsu M, Kousky V, Zhu Y, Leetmaa A, Reynolds R, Chelliah M, Ebisuzaki W, Higgings W, Janowick J, Mo K, Ropelewski C, Wang J, Jenne R, Joseph D. 2001. The NCEP–NCAR 50-year reanalysis: Monthly means CD-ROM and documentation. *Bull. Am. Meteorol. Soc.* **82**: 247–267.

Kvamstø NG, Song Y, Seierstad IA, Sorteberg A, Stephenson D. 2008. Clustering of cyclones in the ARPEGE general circulation model. *Tellus A* **60**: 547–556.

Mailier P. 2007. 'Serial clustering of extratropical cyclones', PhD thesis. University of Reading: Reading, UK.

Mailier P, Stephenson D, Ferro C, Hodges K. 2006. Serial clustering of extratropical cyclones. *Mon. Weather Rev.* **134**: 2224–2240.

McNeil AJ, Frey R, Embrechts P. 2005. *Quantitative Risk Management*, *Princeton Series in Finance. Princeton University Press: Princeton, NJ.*

Mumby PJ, Vitolo R, Stephenson DB. 2011. Temporal clustering of tropical cyclones and its ecosystem impacts. *Proc. Natl. Acad. Sci. U.S.A.* **108**: 17626–17630.

Neu U, Akperov MG, Bellenbaum N, Benestad R, Blender R, Caballero R, Cocozza A, Dacre H, Feng Y, Fraedrich K, Grieger J, Gulev S, Hanley J, Hewson T, Inatsu M, Keay K, Kew SF, Kindem I, Leckebusch GC, Liberato MLR, Lionello P, Mokhov II, Pinto JG, Raible CC, Reale M, Rudeva I, Schuster M, Simmonds I, Sinclair M, Sprenger M, Tilinina ND, Trigo IF, Ulbrich S, Ulbrich U, Wang XL, Wernli H. 2013. Imilast: A community effort to intercompare extratropical cyclone detection and tracking algorithms. *Bull. Am. Meteorol. Soc.* **94**: 529–547.

Pinto JG, Zacharias S, Fink AH, Leckebusch GC, Ulbrich U. 2009. Factors contributing to the development of extreme North Atlantic cyclones and their relationship with the NAO. *Clim. Dyn.* **32**: 711–737.

Pinto JG, Bellenbaum N, Karremann MK, Della-Marta PM. 2013. Serial clustering of extratropical cyclones over the North Atlantic and Europe under recent and future climate conditions. *J. Geophys. Res.- Atmos.* **118**: 12476–12485, doi: 10.1002/2013JD020564.

Prabhu NU. 1961. On the ruin problem of collective risk theory. *Ann. Math. Stat.* **32**: 757–764.

Raible CC. 2007. On the relation between extremes of midlatitude cyclones and the atmospheric circulation using ERA40. *Geophys. Res. Lett.* **34**: L07703, doi: 10.1029/2006GL029084.

Raible CC, Della-Marta PM, Schwierz C, Wernli H, Blender R. 2008. Northern Hemisphere extratropical cyclones: A comparison of detection and tracking methods and different reanalyses. *Mon. Weather Rev.* **136**: 880–897.

Rogers JC. 1997. North Atlantic storm track variability and its association to the North Atlantic Oscillation and climate variability of northern Europe. *J. Clim.* **10**: 1635–1647.

Royden HL. 1953. Bounds on a distribution function when its first *n* moments are given. *Ann. Math. Stat.* **24**: 361–376.

Stephenson DB. 2008. *Definition, Diagnosis, and Origin of Extreme Weather and Climate Events*, Vol. 348. Cambridge University Press: New York, NY.

Trigo IF. 2006. Climatology and interannual variability of storm-tracks in the Euro-Atlantic sector: A comparison between ERA-40 and NCEP/NCAR reanalyses. *Clim. Dyn.* **26**: 127–143.

Ulbrich U, Leckebusch GC, Pinto JG. 2009. Extra-tropical cyclones in the present and future climate: A review. *Theor. Appl. Climatol.* **96**: 117–131.

Villarini G, Smith JA, Vitolo R, Stephenson DB. 2013. On the temporal clustering of US floods and its relationship to climate teleconnection patterns. *Int. J. Climatol.* **33**: 629–640.

Vitolo R, Stephenson D, Cook I, Mitchell-Wallace K. 2009. Serial clustering of intense European storms. *Meteorol. Z.* **18**: 411–424.

Whitaker JS, Sardeshmukh PD. 1998. A linear theory of extratropical synoptic eddy statistics. *J. Atmos. Sci.* **55**: 237–258.

Woollings T, Hannachi A, Hoskins B. 2010. Variability of the North Atlantic eddy-driven jet stream. *Q. J. R. Meteorol. Soc.* **136**: 856–868.

Zhang X, Walsh JE, Zhang J, Bhatt US, Ikeda M. 2004. Climatology and interannual variability of Arctic cyclone activity: 1948–2002. *J. Clim.* **17**: 2300–2317.

